INTERNATIONAL JOURNAL FOR NUMERICAL AND ANALYTICAL METHODS IN GEOMECHANICS
Int. J. Numer. Anal. Meth. Geomech., 2001; **25**:109–129

Inelastic constitutive properties and shear localization in Tennessee marble

D. J. Holcomb[1,*] and J. W. Rudnicki[2]

[1]*Sandia National Laboratories†, P.O. Box 5000, MS 0751, Albuquerque NM 87185-0751, U.S.A.*
[2]*Northwestern University, U.S.A.*

SUMMARY

The inelastic response of Tennessee marble is modelled by an elastic plastic constitutive relation that includes pressure dependence of yield, strain-softening and inelastic volume strain (dilatancy). Data from 12 axisymmetric compression tests at confining pressures from 0 to 100 MPa are used to determine the dependence of the yield function and plastic potential, which are different, on the first and second stress invariants and the accumulated inelastic shear strain. Because the data requires that the strain at peak stress depends on the mean stress, the locus of peak stresses is neither a yield surface nor a failure envelope, as is often assumed. Based on the constitutive model and Rudnicki and Rice criterion, localization is not predicted to occur in axisymmetric compression although faulting is observed in the tests. The discrepancy is likely due to the overly stiff response of a smooth yield surface model to abrupt changes in the pattern of straining. The constitutive model determined from the axisymmetric compression data describes well the variation of the in-plane stress observed in a plane strain experiment. The out-of-plane stress is not modelled well, apparently because the inelastic normal strain in this direction is overpredicted. In plane strain, localization is predicted to occur close to peak stress, in good agreement with the experiment. Observation of localization on the rising portion of the stress–strain curve in plane strain does not, however, indicate prepeak localization. Because of the rapid increase of mean stress in plane strain, the stress–strain curve can be rising while the shear stress versus shear strain curve at constant mean stress is falling (negative hardening modulus). Copyright © 2001 John Wiley & Sons, Ltd.

KEY WORDS: shear localization; constitutive properties; marble; plane strain

1. INTRODUCTION

Shear bands and faults are ubiquitous features of brittle rock deformation at a variety of length scales. Despite the prevalence of these features, understanding of their inception remain rudimentary. Laboratory experiments suggest a casual association of localization of deformation

*Correspondence to: D. J. Holcomb, Sandia National Laboratories, P.O. Box 5000, MS 0751, Albuquerque, NM 87185-0751, U.S.A.

†Sandia is a multiprogram laboratory operated by Sandia Corporation, a Lockheed Martin Company, for the United States Department of Energy under Contract DE-AC04-94AL8500.

Contract/grant sponsor: U.S. Department of Energy, Office of Basic Energy Sciences
Contract/grant number: DE-FG02-93ER14344/09

Received 19 June 1999
Revised 6 July 2000

(faulting) with peak stress, but more detailed examination reveals that localization can precede or follow the peak.

Rudnicki and Rice ([1], hereafter abbreviated as RR) have suggested a theory of the inception of localization as a bifurcation or non-uniqueness of the solution for homogeneous deformation. They predict a strong dependence of localization on deformation state. In particular, they predict that localization can occur prepeak for deformation states near deviatoric pure shear and does not occur until well after peak for axisymmetric compression. This prediction is roughly in accord with the true triaxial experiments of Mogi [2,3]. More recently, Wawersik *et al*., [4], Ord *et al*. [5] and Labuz *et al*. [6] have reported observations of localization prior to peak stress in plane strain experiments using Tennessee marble, Gosford sandstone, and Berea sandstone, respectively. Although there have been numerous extensions of the RR approach to different forms of the constitutive relation (e.g., References [7–9], detailed comparison of predictions of localization with observations has been impeded by several factors.

The predictions of RR depend strongly on the constitutive properties of the rock and then inadequate knowledge prevents accurate evaluation of the localization condition. For soils, there have been some attempts to estimate the relevant parameters (e.g., Vardoulakis, 1981; References [10–13],) but applications to rock have typically assumed the parameters are constant (e.g., References [14,15].) In fact, they are stress dependent and evolve with inelastic deformation. Although axisymmetric compression is by far the most common test configuration for rock, it is not ideal for determining the parameters of any constitutive relation that depends on the stress invariants (such as those used by RR and Ottosen and Runesson [7]). Because the mean and deviatoric portions of the stress change simultaneously and in fixed ratio in the axisymmetric compression test, separating the dependence of the constitutive parameters on them requires many tests at different confining pressures and fairly elaborate reprocessing of the data.

Detailed comparison of predictions of localization with observations is also complicated by the well-known deficiency of smooth yield surface, elastic–plastic constitutive models (or any constitutive model in which the ratios of inelastic strain increments are fixed by the current stress state and independent of the direction of the stress increment) in describing the response to abrupt changes in the pattern of deformation. Because, as discussed by RR, localization of deformation in axisymmetric deformation involves an abrupt change, the prediction of localization for this stress state requires severe softening. Rudnicki [14] has argued that severe softening is consistent with observations of localization in some tests on rocks, but localization is frequently observed much closer to peak stress and with lesser rate of softening than required by the prediction.

Because localization in plane strain does not involve such an abrupt change in the pattern of deformation, the weakness of the smooth yield surface formulation is less of a problem. In addition, localization is predicted to occur at positive hardening modulus (though as discussed later in the paper, this cannot be determined simply by observation of the stress–strain curve). Consequently, plane strain is theoretically an attractive configuration for comparison of observations with theory. Unfortunately, the competing requirements of a sample size large enough to maintain reasonably uniform deformation yet small enough so that the out-of-plane constraint does not require excessive force and the need to control an additional degree of freedom make this a more different experimental configuration for rocks than axisymmetric compression. As a result, the available observations are limited.

A further difficulty with evaluating localization predictions in plane strain is that the deviatoric stress state depends on the out-of-plane normal stress (in the direction of the plane strain

constraint). Because this stress changes with the deformation, the deviatoric stress state changes. In contrast, the deviatoric stress state is fixed by the geometry in axisymmetric configurations. Depending on the evolution of this stress, localization may be predicted to occur with positive or negative plastic hardening modulus. Furthermore, as discussed in more detail in the paper, the sign of the hardening modulus cannot be determined simply by observation of the stress–strain curve in plane strain. As we demonstrate with a simple example, the hardening modulus may be negative while the stress–strain curve is rising. Consequently, inspection of the stress–strain curve is not sufficient to determine whether localization occurs prepeak (in the sense of positive hardening modulus), as has been reported by Wawersik *et al.* [4], Ord *et al.* [5] and Labuz *et al.* [6].

In this paper, we attempt to overcome some of these difficulties. In particular, we synthesize the results of a dozen axisymmetric compression tests to extract a detailed implementation of the constitutive framework used by RR, the parameters entering the localization condition and their dependencies on stress and inelastic deformation. The resulting constitutive relation is then used to predict the response for plane strain. Conditions for localization of deformation derived by RR are evaluated for both plane strain and axisymmetric compression.

2. THEORETICAL BACKGROUND

2.1. Constitutive framework

The constitutive framework used here is that of RR, who generalized the type of relation used for metal plasticity. In particular, they included mean stress dependence of the yield condition and inelastic volume change. This framework is the most general of the class of rate-independent, smooth yield surface elastic plastic models with yield condition and plastic potential depending on the first and second stress invariants. Although, in principal, dependence on the third invariant could be included, our data do not meaningfully constrain this dependence.

The yield condition is the surface in the space of stress components σ_{ij} that is the boundary of those stress states for which the response is elastic; for stress states on the yield surface, the response is inelastic. In general, the yield surface is not fixed but evolves with one or more parameters that characterize accumulated non-elastic (or plastic) deformation. Here, that parameter is taken to be the accumulated plastic shear strain

$$\bar{\gamma}^{\mathrm{p}} = \int \sqrt{(2\,\mathrm{d}e_{ij}^{\mathrm{p}}\,\mathrm{d}e_{ij}^{\mathrm{p}})} \tag{1}$$

where the repeated subscript implies summation and $\mathrm{d}e_{ij}^{\mathrm{p}}$ is the deviatoric part of the inelastic strain increment

$$\mathrm{d}e_{ij}^{\mathrm{p}} = \mathrm{d}\varepsilon_{ij}^{\mathrm{p}} - \frac{1}{3}\delta_{ij}\,\mathrm{d}e^{\mathrm{p}} \tag{2}$$

δ_{ij} ($= 1$, if $i = j$, $= 0$, if $i \neq j$) is the Kronecker delta, and $\mathrm{d}e^{\mathrm{p}} = \mathrm{d}\varepsilon_{kk}^{\mathrm{p}}$. We also decompose the stress into a deviatoric part s_{ij} and a mean normal contribution σ

$$\sigma_{ij} = s_{ij} + \sigma\delta_{ij} \tag{3}$$

where $\sigma = (\frac{1}{3})\sigma_{kk}$. We assume that the yield condition has the following form

$$\bar{\tau} - f(\sigma, \bar{\gamma}^{\mathrm{p}}) = 0 \tag{4}$$

where $\bar{\tau} = \sqrt{(\frac{1}{2}s_{ij}s_{ij})}$ is the equivalent shear stress. The consistency condition ensures that the stress state remain on the yield surface for continuing inelastic deformation

$$\mathrm{d}\bar{\tau} - \mu\,\mathrm{d}\sigma - h\,\mathrm{d}\bar{\gamma}^{\mathrm{p}} = 0 \tag{5}$$

where $\mu(\sigma, \bar{\gamma}^{\mathrm{p}}) = \partial f/\partial\sigma$ is a friction coefficient, and $h(\sigma, \bar{\gamma}^{\mathrm{p}}) = \partial f/\partial\bar{\gamma}^{\mathrm{p}}$ is a plastic hardening modulus.

The flow rule specifies expressions for the plastic portion of the strain increments

$$\mathrm{d}\varepsilon_{ij}^{\mathrm{p}} = \frac{\partial g}{\partial\sigma_{ij}}\,\mathrm{d}\lambda \tag{6}$$

where $g = \bar{\tau} - g(\sigma, \bar{\gamma}^{\mathrm{p}})$ is the plastic potential function and $\mathrm{d}\lambda \geqslant 0$. Taking the deviatoric part of (6) and substituting for the plastic potential yields

$$\mathrm{d}e_{ij}^{\mathrm{p}} = \mathrm{d}\,\lambda\,\frac{s_{ij}}{2\bar{\tau}} \tag{7}$$

Using (7) in (1) reveals that $\mathrm{d}\lambda = \mathrm{d}\bar{\gamma}^{\mathrm{p}}$ and the inelastic volume strain can be written as

$$\mathrm{d}e^{\mathrm{p}} = -\,\beta\,\mathrm{d}\bar{\gamma}^{\mathrm{p}} \tag{8}$$

where $\beta(\sigma, \bar{\gamma}^{\mathrm{p}}) = \partial g/\partial\sigma$ (and the minus sign appears because stresses and strains are taken to be positive in compression). From the consistency condition (5), the increment in accumulated plastic shear strain is given by

$$\mathrm{d}\,\bar{\gamma}^{\mathrm{p}} = \frac{\mathrm{d}\bar{\tau} - \mu\,\mathrm{d}\sigma}{h(\sigma, \bar{\gamma}^{\mathrm{p}})} \tag{9}$$

Since $\mathrm{d}\,\bar{\gamma}^{\mathrm{p}} \geqslant 0$, (9) applies for increments tending to make $\mathrm{d}\bar{\tau} > \mu\,\mathrm{d}\sigma$ in the hardening regime ($h > 0$); for increments tending to made $\mathrm{d}\bar{\tau} \leqslant \mu\,\mathrm{d}\sigma$ ($h > 0$), $\mathrm{d}\bar{\gamma}^{\mathrm{p}} = 0$, and the material unloads elastically. In the softening regime, $h < 0$, and the inequalities are reversed. Substituting for $\bar{\tau}$ and σ, and recombining the deviatoric and volume plastic strain increments yields

$$\mathrm{d}\varepsilon_{ij}^{\mathrm{p}} = \frac{1}{h}\left(\frac{s_{ij}}{2\bar{\tau}} - \frac{1}{3}\,\beta\delta_{ij}\right)\left(\frac{s_{kl}}{2\bar{\tau}} - \frac{1}{3}\,\mu\,\delta_{kl}\right)\mathrm{d}\sigma_{kl} \tag{10}$$

The total strain increment is the sum of (10) and an elastic increment. For isotropic elasticity the latter is

$$\mathrm{d}\,\varepsilon_{ij}^{\mathrm{e}} = \frac{1}{2G}\left(\mathrm{d}\sigma_{ij} - \frac{v}{1+v}\,\mathrm{d}\sigma_{kk}\delta_{ij}\right) \tag{11}$$

where G is the shear modulus and v is Poisson's ratio. Figure 1 (left) shows the geometric interpretation of h in a sketch of the shear stress versus shear strain at constant mean stress. Figure 1 (right) shows that μ is the local slope of the yield surface in the space $\bar{\tau}$ versus σ and that the plastic strain increment vector $(\mathrm{d}e^{\mathrm{p}}, \mathrm{d}\bar{\gamma}^{\mathrm{p}})$ would be perpendicular to the yield surface if β, the negative of the ratio of the volume and shear plastic strain increments, were equal to μ.

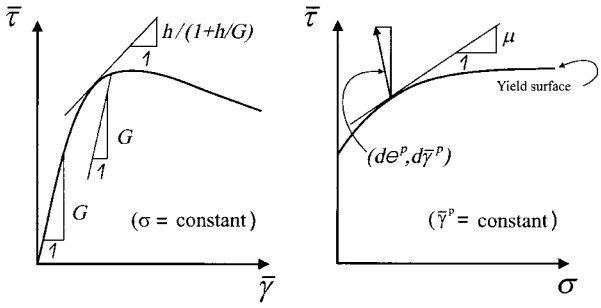

Figure 1. Geometric interpretation of the parameters h (left) and β and μ (right). The slope of the vector $(\mathrm{d}e^{\mathrm{p}}, \mathrm{d}\bar{\gamma}^{\mathrm{p}})$ is $-\beta$.

2.2. Shear localization

RR proposed that faulting could be described as bifurcation from homogeneous deformation. That is, they examined the conditions for which non-uniform deformation in a planar band was an alternative to homogeneous deformation. Formation of the band was required to be consistent with a continuous velocity field and equations expressing continuing equilibrium. These requirements result in a condition depending on the parameters of the constitutive relation and the orientation of the band. Then RR determined the orientation of the band for which this condition is first met. For the constitutive framework introduced in the preceding section, this condition can be expressed as a critical value of the hardening modulus at which localization is first possible. The result is

$$\frac{h_{\mathrm{cr}}}{G} = \frac{(1+\nu)}{9(1-\nu)}(\beta-\mu)^2 - \frac{1}{2}(1+\nu)\left[N + \frac{1}{3}(\beta+\mu)\right]^2 \tag{12}$$

where μ, β, G and ν are as defined earlier and N is the negative of the intermediate principal deviatoric stress divided by $\bar{\tau}$ (using the convention that compressive stresses are positive). As discussed in more detail by RR, expression (12) neglects terms of order $\bar{\tau}/G$; typically, these are small.

The parameter N specifies the deviatoric stress state and ranges from $-1/\sqrt{(3)}$ for axisymmetric extension, through 0 for deviatoric pure shear to $1/\sqrt{(3)}$ for axisymmetric compression. The Lode angle defined as

$$\theta = \frac{1}{3}\arcsin\left\{-\frac{27}{2}\frac{J_3}{(3J_2)^{3/2}}\right\}$$

where $J_2 = \bar{\tau}^2$ and $J_3 = \det(s_{ij})$ are the second and third invariants of the deviatoric stress, can be expressed in terms of N as

$$\theta = \frac{1}{3}\arcsin\left\{\frac{3\sqrt{(3)}}{2}N(1-N^2)\right\}$$

Interestingly, result (12) depends on the third invariant although the constitutive relation does not. This dependence arises from the kinematic requirement that the difference between the localized velocity field and the homogeneous field be a combination of simple shear and uniaxial strain relative to the band.

The maximum value of h_{cr} occurs for $N = -(\beta + \mu)/3$. If $\mu \neq \beta$, the maximum value of h_{cr} is positive. The value of N evolves during plane strain, but for an incompressible material, $N = 0$ for plane strain. For $N = -\beta/3$, the intermediate principal value of the inelastic strain rate is zero and, to the neglect of elastic strains, this corresponds to plane strain.

RR evaluate condition (12) for various constant values of N, μ and β, as have a number of others, but, in general, these parameters evolve during a program of loading.

3. IMPLEMENTATION FOR TENNESSEE MARBLE

To implement the constitutive framework, it is necessary to choose a specific yield function $f(\sigma, \bar{\gamma}^p)$ and plastic potential $g(\sigma, \bar{\gamma}^p)$ (or, equivalently, the dependence of the dilatancy factor on σ and $\bar{\gamma}^p$). A form that is simple, yet suffices to describe the Tennessee marble data, is the following:

$$\bar{\tau} = \tau_0 + f_1(\bar{\gamma}^p, \sigma) + f_2(\sigma) \tag{13}$$

where

$$f_1(\bar{\gamma}^p, \sigma) = (h_0 + h_\infty)\gamma_0^p(\sigma) \arctan\left(\frac{\bar{\gamma}^p}{\gamma_0^p(\sigma)}\right) - h_\infty \bar{\gamma}^p \tag{14}$$

and

$$f_2(\sigma) \sim \mu_0 \min(\sigma, \sigma_0) \tag{15}$$

represents the initial yield surface and its mean stress dependence. In (13)–(15), τ_0, h_0, h_∞, μ_0, and σ_0 are positive constants. The normalizing strain $\gamma_0^p(\sigma)$ is assumed to depend linearly on the mean stress

$$\gamma_0^p(\sigma) = \gamma_{00} + \gamma_{01}\sigma \tag{16}$$

The hardening modulus and friction coefficient can be derived using (13) and the expressions following (5). The results are

$$\begin{aligned} h(\bar{\gamma}^p, \sigma) &= \frac{h_0 + h_\infty}{1 + [\bar{\gamma}^p/\gamma_0^p(\sigma)]^2} - h_\infty \\ \mu(\bar{\gamma}^p, \sigma) &= \mu_0 \mathbf{H}(\sigma_0 - \sigma) \\ &\quad + \gamma_{01}(h_0 + h_\infty)\left\{\arctan\left(\frac{\bar{\gamma}^p}{\gamma_0^p(\sigma)}\right) - \frac{\bar{\gamma}^p/\gamma_0^p(\sigma)}{1 + [\bar{\gamma}^p/\gamma_0^p(\sigma)]^2}\right\} \end{aligned} \tag{17}$$

where $H(s)$ is the Heaviside step function. Because $h(0, \sigma) = h_0$ rather than becoming unbounded, the slope of the shear stress versus shear strain curve (at constant σ) is discontinuous at $\bar{\gamma}^p = 0$. The actual transition from purely elastic behavior is more gradual but this feature is inconsequential.

At peak shear stress, $h = 0$, and from (17) the equivalent plastic strain at peak shear stress ($\bar{\gamma}^{peak}$), is found to be

$$\bar{\gamma}^{peak}(\sigma) = \sqrt{h_0/h_\infty}\,\bar{\gamma}_0^p(\sigma) \tag{18}$$

Because the equivalent plastic shear strain at peak shear stress depends on the mean stress, the locus of the peak shear stress in the $\bar{\tau}$ versus σ plane is not a yield surface as is commonly assumed. The peak shear stress, for constant mean stress, is given by

$$\bar{\tau}_{\mathrm{p}} = \bar{\tau}_{\mathrm{p}}^{0} + T\sigma \tag{19}$$

where

$$\bar{\tau}_{\mathrm{p}}^{0} = \tau_0 + \gamma_{00}\{(h_0 + h_\infty)\arctan\sqrt{(h_0/h_\infty)} - h_\infty\sqrt{(h_0/h_\infty)}\}$$

and

$$T = \mu_0\mathbf{H}(\sigma_0 - \sigma) + \gamma_{01}\{(h_0 + h_\infty)\arctan\sqrt{(h_0/h_\infty)} - h_\infty\sqrt{(h_0/h_\infty)}\}$$

Figure 2 illustrates the graphical interpretation of the parameters. Figure 2 (left panel) sketches the shear stress $\bar{\tau}$ as a function of the equivalent plastic shear strain $\bar{\gamma}^{\mathrm{p}}$ for constant values of the mean stress σ. Figure 2 (right panel) sketches yield surfaces (surfaces of constant $\bar{\gamma}^{\mathrm{p}}$) in the $\bar{\tau}$ versus σ plane.

In order to derive an expression for the dilatancy factor we write the accumulated plastic volume strain as $e^{\mathrm{p}} = E(\bar{\gamma}^{\mathrm{p}}, \sigma)$. Because e^{p} depends on stress path, it cannot, in general, be represented in such a functional form. The introduction of E is, however, simply a device for representing the data for the particular stress path of axisymmetric compression and only the increments of plastic strain enter the constitutive formulation. An increment of inelastic volume strain is given by

$$\mathrm{d}e^{\mathrm{p}} = \frac{\partial E}{\partial \bar{\gamma}^{\mathrm{p}}}\mathrm{d}\bar{\gamma}^{\mathrm{p}} + \frac{\partial E}{\partial \sigma}\mathrm{d}\sigma$$

The negative of the coefficient in the first term is the dilatancy factor. (Note that E is related to the flow potential by $\partial g/\partial\sigma = -\partial E/\partial\bar{\gamma}^{\mathrm{p}}$.) The second term represents inelastic compaction, that is, inelastic volume strain due to mean stress. Here this term is deleted since the RR formulation assumes that all inelastic volume change is related to inelastic shearing. This assumption is consistent with data on low-porosity rocks but a more general representation would include a term representing inelastic compaction. There is, however, no reason to expect that the coefficients of the two terms can necessarily be expressed as partial derivatives of a single function.

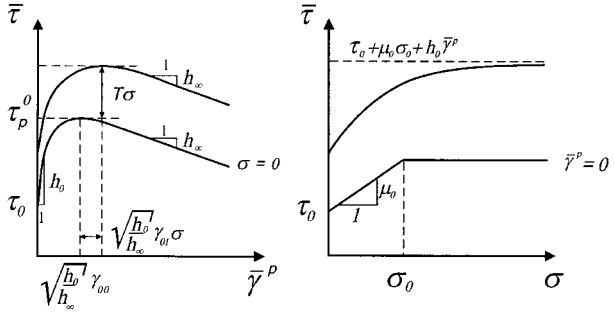

Figure 2. Key parameters used in modelling the dependence of μ and h on $\bar{\gamma}^{\mathrm{p}}$ (left) and σ (right).

Table I. Numerical values of coefficients

Parameter	Value
h_0	68.27 GPa
h_∞	0.62 GPa
μ_0	0.39
γ_{00}	3.84×10^{-5}
γ_{01}	5.26×10^{-6} MPa
σ_0	68.57 MPa
τ_0	34.72 MPa
β_0	0.43
β_∞	1.49
c_0	2.37×10^{-4}
c_1	3.71×10^{-3}
B	3.32×10^{-2}

A form of the function $E(\bar{\gamma}^p, \sigma)$ suggested by the data is

$$E(\bar{\gamma}^p, \sigma) = [\beta_\infty - B(\sigma/\sigma_0)]\bar{\gamma}^p + (\beta_\infty - \beta_0)c(\sigma)\arctan\left\{\frac{\bar{\gamma}^p}{c(\sigma)}\right\} \tag{20}$$

where

$$c(\sigma) = c_0 - c_1(\sigma/\sigma_0)$$

and $\beta_0, \beta_\infty, c_0, c_1$, and B are constants. The dilatancy factor is given by

$$\beta(\sigma, \bar{\gamma}^p) = -B(\sigma/\sigma_0) + \beta_\infty - \frac{\beta_\infty - \beta_0}{1 + (\bar{\gamma}^p/[c_0 - c_1(\sigma/\sigma_0)])^2}$$

Thus, the dilatancy factor at zero equivalent plastic shear strain ($\bar{\gamma}^p = 0$) is $\beta_0 - B(\sigma/\sigma_0)$ and β approaches $\beta_\infty - B(\sigma/\sigma_0)$ as $\bar{\gamma}^p \to \infty$. Figure 3 sketches β (left panel) and $e^p = E$ (right panel) as function of $\bar{\gamma}^p$ for two values of mean stress. Numerical values for these coefficients are given in Table I.

4. DETERMINATION OF MODEL PARAMETERS

Determining the model parameters is a several-step process, beginning with acquisition of a data set, determining, τ, σ, $\bar{\gamma}^p$ and e^p and finally fitting the model parameters to the processed data set. Experimental results from conventional triaxial tests on 5 cm diameter cylinders of Tennessee marble were analysed to obtain $\bar{\gamma}^p$ and e^p. The elastic strains were removed by using a least-squares fitting process to simultaneously determine G and ν from the initial portions of the loading curves. In general for rocks, G and ν may change with mean stress and inelastic deformation. For Tennessee marble, the change is negligible. Stress–strain curves for axisymmetric compression of Tennessee marble in Figure 3 of Wawersik and Faithurst [16] show virtually no variation of initial Young's modulus for confining pressures from 0 to 50 MPa and the same is

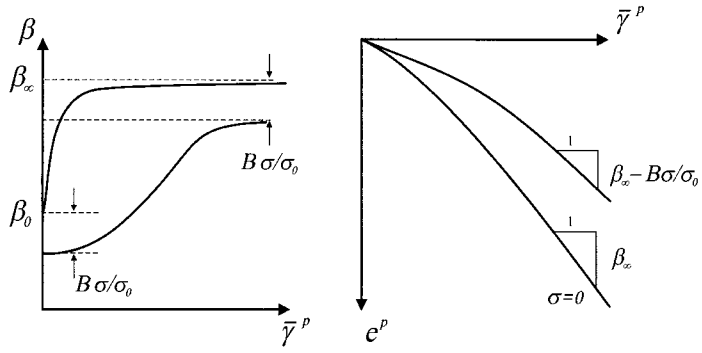

Figure 3. β as a function of $\bar{\gamma}^p$ (left) and parameters used in the model (right).

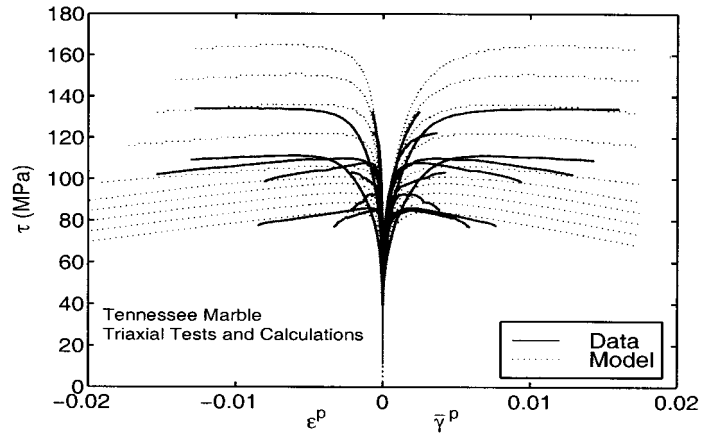

Figure 4. Comparison of experimental results used to derive the model parameters with the stresses and strains calculated from using the fitted parameters.

true of the specimens tested here. Unloading moduli for unconfined compression (inferred from Figure 4 of Wawersik and Fairhurst [16] do show some decrease with deformation, but only after deformation has progressed well into the postpeak regime. For example, the unloading modulus decreases by about 10 per cent of the initial value when the stress falls to about 75 per cent of the peak value. Consequently, $G = 30$ GPa and $\nu = 0.34$ were assumed constant.

Twelve experiments, conducted at confining pressures from 0 to 100 MPa, were analysed to produce a data set consisting of values for $\bar{\tau}$, σ, $\bar{\gamma}^p$ and e^p. Our goal was to find values for the model parameters listed in Table I which would minimize a suitable measure of the difference between the experimental and modeled values for $\bar{\tau}$ and e^p. A simplex algorithm was used to solve the minimization problem.

Although the downhill simplex algorithm is not particularly efficient, it is appealing for solving minimization problems because it is easy to implement, requires no differentiation and readily allows inclusion of constraints. Nelder and Mead [17] first described the downhill simplex

method, but a more accessible reference may be *Numerical Recipes* ([18], pp. 289). A simplex in two dimensions is a triangle (three vertices), in three dimensions a tetrahedron (four vertices) and so on to an object with $N + 1$ vertices in N dimensions corresponding to the N unknowns of the minimization problem. Each vertex corresponds to an N-tuple of possible values for the sought-after set of parameters that minimize the appropriate measure of error. In our problem, the unknowns are the 12 parameters listed in Table I. The error function to be minimized was L2 norm of the difference between the experimental values of $\bar{\tau}$ or e^{p} and the corresponding values calculated from Equations (13) and (20). The procedure was implemented with the constraint that $\mu < \sqrt{(3)}$. (Since $\sqrt{(3)}$ is the slope of the $\bar{\tau}$ versus σ trajectory in a conventional triaxial test, for values of $\mu > \sqrt{(3)}$ the mean stress increases too rapidly to allow inelastic deformation).

To begin the process, $N + 1$ starting vectors are chosen that define the vertices of the initial simplex in the N-dimensional space of unknowns. At each vertex, the error function is evaluated, by calculating the value of $\bar{\tau}$ for the several hundred experimental data points, using the experimental values of $\bar{\gamma}^{\mathrm{p}}$ and σ and the N-tuple of parameter values that are the vertex coordinates. Then the simplex shape is modified to move it towards regions of the parameter space that give lower values for the error functions. The simplest movement is away from the vertex with the highest value of the error function, accomplished by reflecting that vertex across to the other side of the simplex. In two dimensions the process is easily visualized as an amoeba-like series of stretchings, contractions and crawling that moves the triangular simplex as a whole towards smaller and smaller error values. When a minimum lies within the simplex, further movement ceases to lower the error and a series of contractions are instituted that shrink the simplex until some specified convergence criterion is met. There is no guarantee that the minimum is not just a local minimum, so it is standard practice to restart the simplex at a different region of the parameter space and see if the same minimum is found.

Two separate minimizations were carried out: one to obtain the parameters necessary to describe the hardening modulus and the friction coefficient and the other for the parameters in the model of the dilatancy factor. As Figures 2 and 3 show, the parameters could be found by choosing values from individual tests at special points. However, fitting all of the triaxial test data avoided overemphasizing any one test or portion of a test. Another approach would have been to model the hardening modulus, friction factor and dilatancy parameter directly. This would have required differentiating the experimental stress–strain curves, which would inevitably produce a noisy data set to be fit. By modeling $\bar{\tau}$ and e^{p} as functions of $\bar{\gamma}^{\mathrm{p}}$ and σ, we were able to carry out the differentiations required to obtain h, μ, and β on smooth analytic functions.

Once determined, the parameters in Table I can be used to calculate the response for different stress paths by substituting the expressions for μ, β and h into (10) and numerically integrating. To accomplish the integration, the constitutive equations were specialized to axisymmetric compression and written as a system of ordinary differential equations with the total component ε_{11} chosen as the independent variable. These can be solved by any standard method augmented by a Newton–Raphson iteration to ensure that the stress state stays sufficiently close to the yield surface (4). The accuracy of the resulting solutions was checked by comparison with the output of single-element calculations using a material sub-routine written to use this constitutive relation in the commercial finite element code ABAQUS (see References [19,20]).

A comparison of experiment and calculations for all of the fitted triaxial tests is shown in Figure 4. This comparison confirms the suitability of assuming constant G and E. The data show a variability typical of natural materials. For example, diminished softening with increasing mean stress would be expected and is generally, but not exclusively, observed.

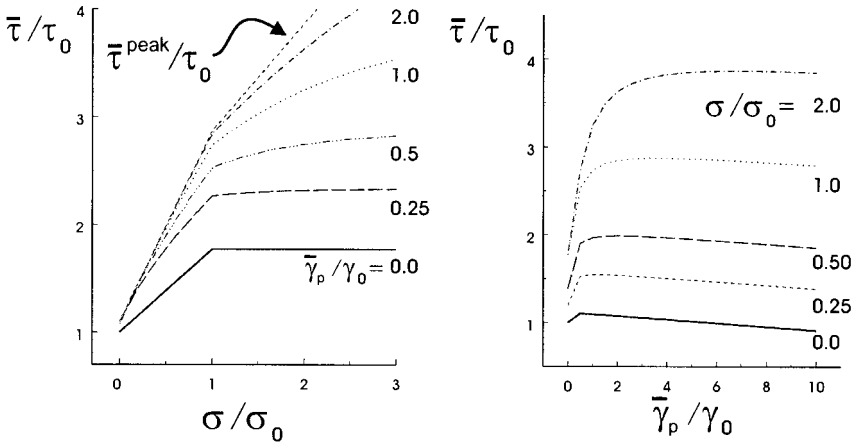

Figure 5. Results of modelling yield surfaces (a) and shear stress as a function of plastic shear strain $\bar{\gamma}^p$ at constant mean stress (b). The curve marked $\bar{\tau}^{peak}/\tau^0$ in (a) shows peak stress as a function of σ. Numerical results show the locus of peak stresses crosses the yield surfaces, indicating that the locus of peak stresses is not a yield surface.

Calculated yield surfaces for several values of $\bar{\gamma}^p$ are shown in Figure 5(a) and shear stress versus shear strain at several values of mean stress are shown in Figure 5(b). Also shown in Figure 5(a) is the peak stress as a function of mean stress. Although it is not apparent at the scale of the figure, the curve of peak stress cuts across the yield surfaces and, hence, as noted earlier, is not itself a yield surface. This result does not depend on the particular constitutive model used here: because the measured plastic shear strains at peak stress depend on the mean stress, any model consistent with this feature of the data would give essentially the same result.

5. LOCALIZATION UNDER AXISYMMETRIC COMPRESSION

Using the constitutive relations described earlier, we have examined the localization criterion (Equation (12)) for axisymmetric compression tests. Figure 6 shows the evolution of the hardening modulus (17) and the critical hardening modulus needed for localization (12) for $\sigma_{22} = \sigma_{33} = 5$ and 20 MPa. Results for other confining stresses are similar: the hardening modulus decreases but never becomes sufficiently negative to equal the critical value. The minimum attainable value of h in the constitutive model is negative ($-h_\infty$, see Equation (17)). The value of the critical hardening modulus predicted for localization h_{cr} is also negative. But the magnitude of h_{cr} is predicted to be a substantial fraction of the elastic shear modulus G, and, thus, is far more negative than the possible values for h. Because post-test examination of the samples revealed localization in the form of through-going fractures, the predictions for localization based on (12) are not accurate.

One possible reason for this discrepancy is that the value of h_∞ may not be well constrained by the data. This value reflects the slopes of the stress–strain curves well into the post peak regime, that is, for large $\bar{\gamma}^p$. Although most of the tests extended past peak stress, several, especially at the higher confining pressures did not (Figure 4). Because the value of h_∞ does fit the data, the model

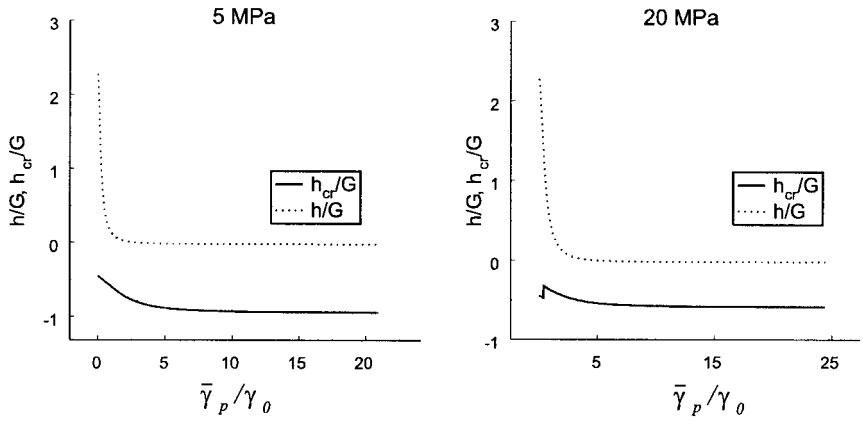

Figure 6. Calculation of the critical hardening modulus and the material hardening modulus, plotted as a function of normalized plastic shear strain for triaxial load paths at confining pressures $\sigma_{22} = \sigma_{33} = 5$ and 20 MPa. The graphs show that the localization criterion is never met. Plot is for $G = 30$ GPa and $\nu = 0.34$.

stress–strain curves eventually reach a peak at all confining pressures. We would expect, however, that for high confining pressures, h might never become negative, even for large $\bar{\gamma}^{\mathrm{p}}$, reflecting a brittle-to-ductile transition [15]. If additional data were available at the higher confining pressures, this feature could be included by introducing an additional pressure dependence in the slope for large $\bar{\gamma}^{\mathrm{p}}$.

Another, more significant reason for the failure to predict localization in axisymmetric compression is related to the structure of the constitutive relation. As discussed by RR (and by Rice [21]), the strongly negative values of h_{cr} predicted for localization in axisymmetric compression are related to the overly stiff response of a smooth yield surface model to the abrupt change in the pattern of deformation. Localization into a planar band requires the difference between the strain rates of the localized and uniform fields to vanish in a plane [21]. When the pre-localization field is axisymmetric, this kinematic condition for the formation of a band requires an abrupt change in the ratio of components of inelastic strain increments. RR note that the overly stiff response to this abrupt change predicted by smooth yield surface models is alleviated by models that have a vertex at the current stress point, a feature predicted for a wide range of microstructural models [22]. Evidence for the formation of a yield surface vertex has been observed in compression-torsion tests on Tennessee marble [23]. To approximate the response at a yield surface vertex RR introduced an additional 'vertex modulus' h_1. The resulting modified constitutive relation could be interpreted as a type of deformation plasticity [24] and h_1 could, under certain circumstances, be regarded as a secant modulus. RR showed that this modification reduced the magnitude of the negative values of h at which localization was predicted for axisymmetric compression, roughly by a factor of h_1/G.

Unfortunately, there is virtually no independent evidence of the appropriate values of h_1 in rocks, although the discrepancy between prediction and observation of localization in axisymmetric compression has sometimes been regarded as indirect evidence for the presence of vertex or non-coaxiality effects. The sole exception of which we are aware is the work of Olsson [25], who measured various shear moduli in compression-torsion tests on Tennessee marble at

a confining pressure of 60 MPa. The modulus Olsson labeled G^* corresponds directly to RR's h_1. Olsson's Figure 5 shows a decrease of G^*/G (corresponding to h_1/G) to about 0.20. Estimates from the results of RR (1975) suggest that values of $h_1/G \approx 0.1$, a factor of two smaller, are required to reduce h_{cr} to $-h_\infty$. Without better observational evidence to constrain the form and magnitude of the response at a vertex, accurate predictions will be difficult.

6. SIMULATIONS OF PLANE STRAIN

An exacting test of the constitutive model is to compare its predictions with data from a significantly different deformation state. Consequently, we have used the constitutive relation to simulate the results of a plane strain test (zero strain in the x_2 direction) with constant lateral compressive stress ($\sigma_{33} = 20$ MPa). Because localization from a plane strain deformation state does not require so abrupt a change of inelastic strain-rate direction as axisymmetric deformation, plane strain is also a favourable deformation mode for comparison of predictions and observations of localization.

6.1. Constitutive response

Figure 7 compares the predicted (dashed lines) and measured values (solid lines) for the stresses, σ_{11} and σ_{22} versus ε_{11}. Because of the more rapid increase of mean stress in plane strain, the hardening is augmented, by comparison with that in axisymmetric compression. Note that the test included unloading loops (the small ticks off the main load line) that were not included in the modelling. In order to reach predicted localization, the model calculations were extended to larger values of strain than were achieved in the tests.

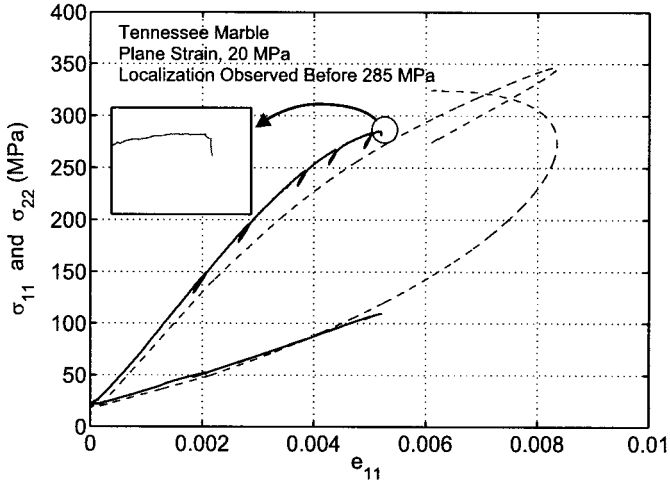

Figure 7. Comparison of the calculated (dashed lines) and experimental (solid lines) maximum compressive (σ_{11}) and intermediate (σ_{22}) stresses as a function of total strain ε_{11} for a plane strain test on Tennessee marble. An enlarged view of the end of the test shows localization occurring.

The elastic constants obtained from the plane strain tests and used to plot the model results in Figure 7, $G = 22$ GPa and $\nu = 0.25$, differed slightly from those obtained for axisymmetric compression tests, $G = 30$ GPa and $\nu = 0.34$. As noted earlier, the latter are consistent with values measured by Wawersik and Fairhurst [16]. The difference exceeds what would be expected from material variation, especially for Tennessee marble which has proven to be very consistent in its properties as a function of different blocks of starting material. Furthermore, neither the axisymmetric compression tests nor the plane strain tests give any indication of significant dependence of elastic constants on stress, or inelastic deformation. It is likely that the added complexity of indirectly measuring strains on samples in the plane strain apparatus has introduced an error. Fortunately the error is irrelevant to the considerations here: the model is based entirely on the results of the axisymmetric tests and our focus is the inelastic response. Use of the different constants in plane strain only facilitates comparison of the predicted and observed responses; alternatively, the plastic strains could have been compared with those determined from the data using the measured values of G and ν.

Modelling reproduced the behaviour of ε_{11} well, but the calculated variation of ε_{22} differs significantly from that measured. Experimental data indicate a nearly linear response of σ_{22} as would be expected if the material remained elastic. Figure 8 confirms that the measured elastic strain along the out-of-plane axis was small. Because total strain, $\varepsilon_{22} = \varepsilon_{22}^{e} + \varepsilon_{22}^{p}$, was constrained to be exactly zero (plane strain), $\varepsilon_{22}^{e} = -\varepsilon_{22}^{p}$. Thus a small elastic strain component requires an equally small plastic strain component of opposite sign. In contrast to the experimental results, the modelled results for ε_{22} in Figure 8 show a large elastic strain, requiring an equally large plastic strain. The large elastic strain in turn forced the modelled σ_{22} to increase more rapidly than in the experiment.

There are several possible reasons for this discrepancy. One is that any dependence of the third stress invariant has been neglected in the constitutive formulation. In principal, this dependence

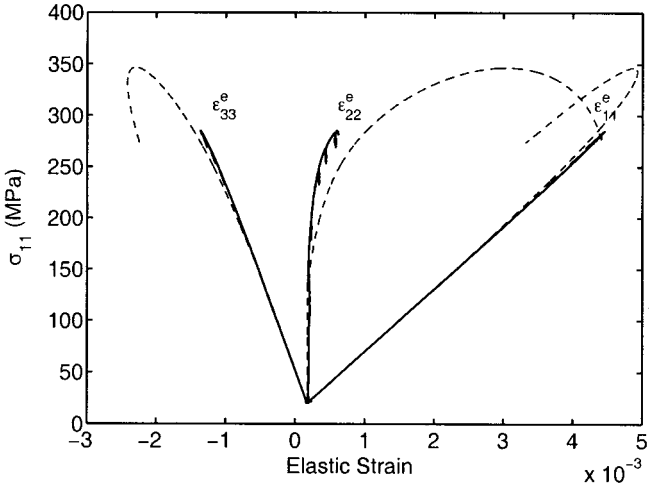

Figure 8. Comparison of calculated (dashed lines) and experimental (solid lines) elastic strain versus σ_{11} for a plane strain test on Tennessee marble. The in-plane strain components (ε_{11}^{e} and ε_{33}^{e}) were well described by the model, but the out-of-plane component (ε_{22}^{e}) was not.

could be estimated by comparison of stress–strain curves in plane strain and axisymmetric compression. But, the number of plane strain tests was small and the good agreement of the observations and calculations for σ_{11} suggests that this dependence is not likely to be severe. Another possibility is that the elasticity is anisotropic, perhaps, in part, due to the preferential growth of cracks perpendicular to the minimum principal stress.

Although the two factors in the preceding paragraph may contribute to the discrepancy between the observed and predicted values of σ_{22}, we believe that it is primarily caused by the way in which dilatancy is modelled (Equation (7)): An increment of inelastic deviatoric strain, in any direction, contributes to $d\bar{\gamma}^{\mathrm{p}}$ and causes equal increments of inelastic normal strain in all directions. In actuality, dilatancy in the x_2-direction is likely to be less because shearing occurs principally in the x_1–x_3 plane and because the opening of microcracks in the x_2-direction is suppressed by the increasing normal stress in this direction. Inclusion of this effect would require an anisotropic model and indicates the difficulties of constructing a constitutive model from (even many) results for a single deformation state.

6.2. Localization

Because the plane strain test was controlled in a manner to ensure that stability was maintained as localization was occurring, it was possible to observe what we interpreted to be the occurrence of localization. The test was conducted using servo-hydraulic control of the load frame to maintain the strain rate constant for ε_{33}, the strain in the minimum compressive stress direction. Consequently, the spontaneous decrease (unloading) of σ_{11}, the maximum compressive stress, as ε_{33} continued to increase (see enlarged portion of Figure 7) implies the onset of a process that caused the strain rate in x_3 direction to increase rapidly. Only by reducing σ_{11} and thus its contribution to $\dot{\varepsilon}_{33}$, under the control of the servo-hydraulic system, was it possible to maintain the specified strain rate. Localization is the likely cause of the change in behaviour that occurred at $\sigma_{11} = 285$ MPa.

This observation is compared with the prediction of localization made by plotting the evolution of the hardening modulus (dividing by G) and the evolution of critical hardening modulus (given by (12)) against $\bar{\gamma}^{\mathrm{p}}$ (Figures 9 and enlarged in Figure 10). Model results indicate that the critical hardening modulus was initially negative but increased during the test, resulting in the satisfaction of the localization criterion $h = h_{\mathrm{cr}}$ when h decreased to $h_{\mathrm{cr}} \approx 0$. In contrast, for axisymmetric compression the predicted localization criterion required a large negative h.

The evolution of h_{cr} is due to change of μ, β (Figure 9) and the deviatoric stress state parameter, N, which is plotted against the total axial strain in Figure 11. At the onset of loading, $N \approx 0.3$ as required for the elastic solution to plane strain loading. During the test, N evolves through pure shear ($N = 0$) and towards axisymmetric extension ($N = -1/\sqrt{(3)}$).

Because of the rapid increase of mean stress in plane strain (compared with axisymmetric compression) the sign of the local slope of the stress σ_{11} versus strain ε_{11} curve may be different from the sign of h. Consequently, it is not possible to draw conclusions about the sign of h from the local shape of stress–strain curves at localization in plane strain as was done by Ord *et al.* [5]. They argued that the observation of localization during increasing stress implied that h was positive, i.e. that localization had occurred 'pre-peak'. This argument is valid for constant mean stress tests ($\dot{\sigma} = 0$) and for axisymmetric compression tests for which μ and β are both less than $\sqrt{3}$ (see Equation (10)). For those tests, $h = 0$ implies that the peak shear stress and the peak of the stress–strain curves has been reached. In general, and in particular for plane strain tests, it is

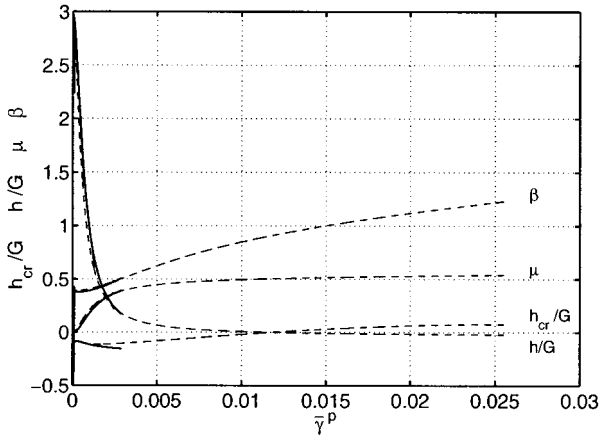

Figure 9. Comparison of calculated (dashed lines) and experimental (solid lines) values of h, h_{cr}, β and μ as a function of $\bar{\gamma}^p$ for a plane strain test on Tennessee marble.

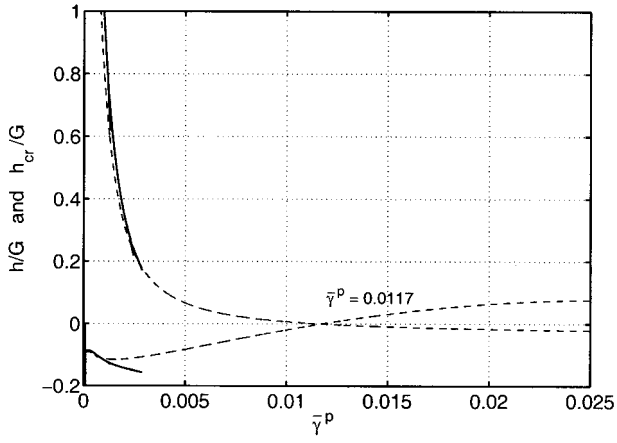

Figure 10. From modelling, localization is predicted to occur for plane strain conditions when $h = h_{cr} = -2.5 \times 10^{-4}$ (dashed lines) at $\bar{\gamma}^p = 0.0117$. This is significantly different from the experimental results (solid lines) which were interpreted to show localization at approximately $h = 0.2$.

not possible to determine the sign of h at any given point by examining stress–strain curves. For example, as Figure 12 shows, at the predicted localization point ($\bar{\gamma}^p = 0.0117$), the shear stress is still increasing, even though $h = -2.5 \times 10^{-4}$ is already slightly negative (see Figure 10). Only by a detailed calculation, similar to the one carried out here, can the value of h be determined, allowing an assessment of whether localization occurred for positive or negative h, that is, in the hardening or softening regime.

The evolving value of N, as indicated in Figure 11, causes a change in the value of h_{cr}, in addition to those due to evolving β and μ. The value of N reflects the stress required to enforce

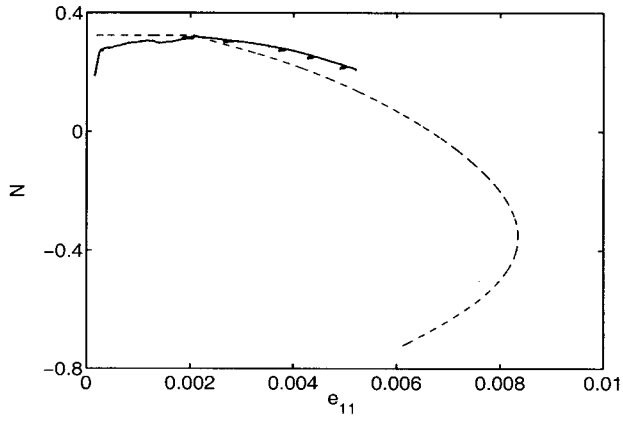

Figure 11. Evolution of N during the course of a plane strain test as a function of ε_{11}, the strain along the maximum compressive stress axis, showing the evolution towards an axisymmetric stress state and back towards pure shear (solid line from experiment, dashed line from model).

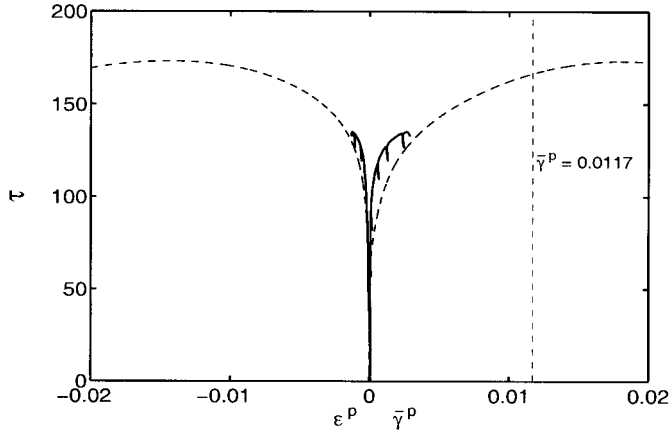

Figure 12. Comparison of calculated (dashed lines) and experimental (solid lines) values for τ versus e^{p} and $\bar{\gamma}^{\mathrm{p}}$ for a plane strain test on Tennessee marble. As a result of changing mean stress, the stress–strain curve appears to show hardening, even though h was already slightly negative, in the softening regime.

plane strain and this stress will, in turn, depend on the constitutive relation. As suggested by Figure 8, the RR model used here overpredicts the out-of-plane inelastic strain and, hence, the out-of-plane elastic strain and stress. Consequently, the predictions of localization are intimately related to the details of the constitutive behaviour. This is not surprising: at the microstructural scale localization actually involves a complicated process of microcrack growth, link-up and interaction; a macroscopic, phenomenological constitutive relation, such as (10) reflects these microstructural processes in only an average way.

6.3. An example

As mentioned in the preceding section, as a result of the rapid increase of mean stress in the plane strain test, the slope of the stress versus strain curve, i.e. σ_{11} versus ε_{11} can be positive while $h < 0$. Because the localization condition is met at $h_{cr} \approx 0$ for the plane strain test on Tennessee marble, the distinction between the sign of the slope of the stress–strain curve and the sign of h is not evident. Consequently, a simpler, constructed example, shown in Figure 13, is used to emphasize this point.

The yield condition is given by

$$\bar{\tau} = \tau_0 - 0.02G\bar{\gamma}^p - 0.7\sigma \tag{21}$$

Thus, h has the constant value $-G/50$, and μ has the constant value 0.7. In addition, we assume that $\beta = 0$ and the lateral confining stress is zero. The resulting pure shear response (constant σ) is bilinear: an elastic portion with slope G until the shear stress reaches τ_0 followed by a descending portion with slope $-G/49$. Similarly, the modelled axial strain response in axisymmetric compression is also bilinear. For Poisson's ratio $\nu = 0.2$, the slope is $E = 2.4G$, until the axial stress reaches $5\tau_0/\sqrt{(3)}$, and then the slope is $-12G/115$.

For plane strain, however, the response is non-linear. As shown in Figure 13(a), even though $h = -G/50 < 0$ as soon as inelastic deformation occurs, the curve of σ_{11} versus ε_{11} continues to

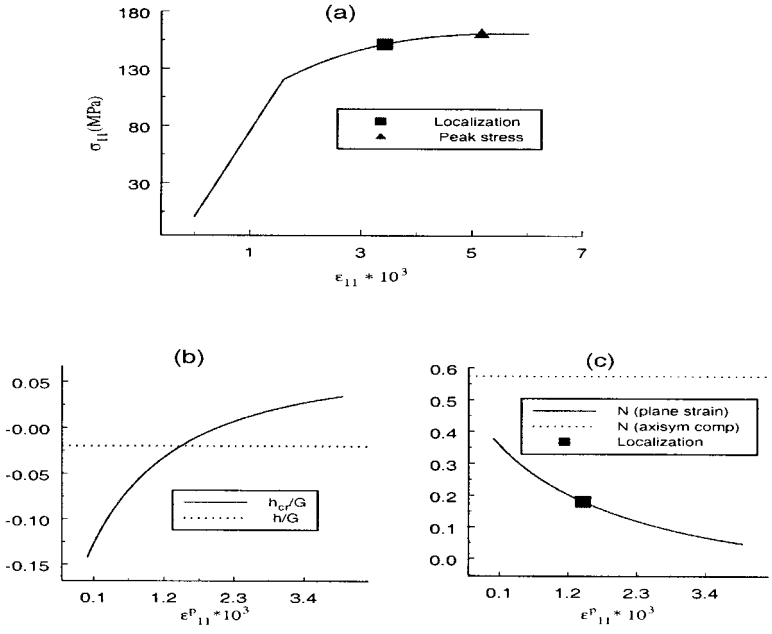

Figure 13. An example showing that h can be negative at localization under plane strain conditions while the apparent hardening in positive. (a) Curve of axial stress (σ_{11}) versus axial strain (e_{11}) for plane strain loading, continues to rise until the peak stress (triangle) even though $h/G = -0.02$. Localization (square) is predicted to occur when h_{cr}/G rises to equal $h/G = -0.02$. (b) Evolution of h_{cr} is due to evolution of N (c) toward pure shear ($N = 0$).

rise until peak load (indicated by the triangle). In this example, $h_{cr}/G = 0.0653$ for deviatoric pure shear ($N = 0$) and -0.3127 for axisymmetric compression. Thus, localization is predicted to occur for deviatoric pure shear but not for axisymmetric compression. For plane strain, h_{cr}/G evolves with deformation (Figure 13(b)) because of the changing value of N (Figure 13(c)). Localization is predicted to occur at the point indicated by the box, when h_{cr} has risen to equal the constant value of $h = -G/50$ (Figure 13(b)). The increase of the critical value of h_{cr} in this case is due entirely to the evolution of the deviatoric stress state from near axisymmetric compression ($N = 1/\sqrt{(3)}$), for which h_{cr} is very negative, towards deviatoric pure shear ($N = 0$), for which h_{cr} is less negative. Thus, observation of localization under rising load in plane strain does not necessarily mean that h is positive.

7. CONCLUSION

Predictions of faulting (shear banding) as a bifurcation from homogeneous deformation, as proposed by RR, are strongly dependent on the constitutive description of homogeneous deformation. The constitutive framework used here, and adopted from RR, is the most general form for a rate-independent, elastic–plastic model with yield function and plastic potential dependent on the first and second stress invariants. Data from 12 axisymmetric tests on Tennessee marble at confining pressures from 0 to 100 MPa were used to determine the specific forms of the yield function and plastic potential and their evolution with the accumulated inelastic shear strain. Because the mean stress and equivalent shear stress (second invariant of the deviatoric stress) change simultaneously and in fixed ratio in axisymmetric compression, this determination required manipulation to extract these dependencies from the test data. A feature that emerges from the data analysis is that the peak stress is not a yield surface as is conventionally assumed This result is model-independent; it will be the case whenever the data indicate that the inelastic strain at peak stress depends on the mean stress. Since the peak stress is, in general, neither a yield surface nor the stress at which localization occurs, the prominence given to this parameter may be more due to its ease of observation than any fundamental significance.

Comparison of the axisymmetric compression stress–strain curves obtained by numerical integration of the resulting constitutive relation with the original test data verified that the relation did adequately reproduce the data. The localization condition, evaluated for the constitutive parameters was, however, never met for axisymmetric compression. The predicted values of the hardening modulus h required for localization are so negative that the modelled axisymmetric tests never soften enough to reach this value. In contrast, post-test examination of the specimens revealed that localization in the form of a fault did occur in most. The discrepancy is likely due to the well-known deficiency of smooth yield surface models to predict the response to abrupt changes in the pattern of strain as occurs in localization in axisymmetric compression. The predictions could be brought into accord with observations by introducing a vertex or non-coaxiality modulus. Unfortunately, except for the compression-torsion experiments of Olsson [25], there appear to be no direct observations that would provide guidance for modelling the response at vertex. In principal, such information could be obtained from micromechanical models, though models that include the complexity of mechanisms that occur in rocks have not yet been developed. Moreover, such a model would need to be calibrated against experiments of the type conducted by Olsson [25] in order to form the basis of reliable predictions.

The constitutive relation determined from the axisymmetric compression experiments was used (again, with numerical integration) to predict the response in plane strain. The predicted response was compared with the results for a plane strain experiment. In principle, there is little reason to expect that the relation determined from axisymmetric compression will describe well the response for a much different deformation state such as plane strain. Nevertheless, the variation of the maximum compression stress with strain agreed satisfactorily with the observations. The out-of-plane stress was, however, modelled less well. Several factors could contribute to this discrepancy but it is primarily due to the way in which dilatancy enters the constitutive relation: inelastic shear strain causes equal dilatancy in all principal directions though normal strain in the constraint direction is likely suppressed.

Careful evaluation of the conditions for localization for plane strain requires including the evolution of the deviatoric stress state. Both the data and the model predictions demonstrated that the deviatoric stress state, as described by N, evolved from near axisymmetry at the onset of inelasticity through deviatoric pure shear toward axisymmetric extension when the condition for localization was met. The condition for localization was met for a value of the hardening modulus that was slightly negative, although the stress–strain curve was still rising. The manner in which the test was controlled made it possible to infer the onset of localization and this occurred at a stress in reasonable agreement with the predicted value. The difference in sign of the hardening modulus and the slope of the stress–strain curve can occur in plane strain because of the rapid increase of mean stress (compared with axisymmetric compression). This point was illustrated by a simple example as it can lead to misinterpretation of results on whether localization occurs with positive or negative hardening modulus.

ACKNOWLEDGEMENTS

Richard Albert provided a careful review of the manuscript and verified some of the calculations using the ABAQUS finite element program (made available from Hibbit, Karlson and Sorenson by means of an academic license).

The example illustrated in Figure 13 was adapted from unpublished finite element calculations of Nigel Higgs.

Financial support was provided by the U.S. Dept. of Energy, Office of Basic Energy Sciences, Geosciences Research Program through a grant to Sandia National Laboratories (DJH) and through Grant No. DE-FG02-93ER14344/09 to Northwestern University (JWR).

REFERENCES

1. Rudnicki JW, Rice JR. Conditions for the localization of deformation in pressure-sensitive dilatant materials. *Journal of the Mechanics and Physics of Solids* 1975; **23**:371–394.
2. Mogi K. Effect of the intermediate principal stress on rock failure. *Journal of Technical Research* 1967; **72**:5117–5131.
3. Mogi K. Effect of the triaxial stress system on the failure of dolomite and limestone. *Tectonophysics*, 1971; **11**:111–127.
4. Wawersik WR, Rudnicki JW, Olsson WA, Holcomb DJ, Chau KT. Localization of deformation in brittle rock: theoretical and laboratory investigations. In *Micromechanics of Failure of Quasi-Brittle Materials*, Shah SP, Swartz SE, Wang ML (eds). Elsevier: New York, 1991; 115–124.
5. Ord A, Vardoulakis I, Kajewski R. Shear band formation in Gosford Sandstone. *International Journal of Rock Mechanics and Mining Sciences* 1991; **28**:397–409.
6. Labuz JF, Dai S-T, Papamichos E. Plane strain compression of rock-like materials. *International Journal of Rock Mechanics and Mining Sciences and Geomechanics Abstract* 1996; **33**:573–584.
7. Ottosen NS, Runesson K. Properties of plastic bifurcation solutions in elasto-plasticity. *International Journal of Solids Structures* 1991; **27**:401–421.

8. Runesson K, Ottosen NS, Perić D. Discontinuous bifurcations of elastic-plastic solutions at plane stress and plane strain. *International Journal of Plasticity* 1991; **7**:99–121.
9. Perić D, Runesson K, Sture S. Evaluation of plastic bifurcation results for plane strain versus axisymmetry. *Journal of Engineering Mechanics ASCE* 1992; **118**:512–524.
10. Vardoulakis I, Goldscheider M, Gudehus G. Formation of shear bands in sand bodies as a bifurcation problem. *International Journal for Numerical and Analytical Methods in Geomechanics* 1978; **2**:99–128.
11. Vardoulakis I. Shear band inclination and shear modulus of sand in biaxial tests. *International Journal for Numerical ad Analytical Methods in Geomechanics* 1980; **4**:103–119.
12. Vardoulakis I, Graf B. Calibration of constitutive models for granular materials using data from biaxial experiments. *Géotechnique* 1985; **35**:299–317.
13. Papamichos E, Vardoulakis I. Shear-band formation in sand according to noncoaxial plasticity model. *Géotechnique* 1995; **45**:131–143.
14. Rudnicki JW. The inception of faulting in a rock mass with a weakened zone. *Journal of Geophysical Research* 1997; **82**:844–854.
15. Frederich JT, Evans B, Wong, T-F, Micromechanics of brittle to plastic transition in Carrara marble. *Journal of Geophysical Research* 1989; **94**:4129–4145.
16. Wawersik WR, Fairhurst C. A study of brittle rock fracture in laboratory compression experiments. *International Journal of Rock Mechanics and Mining Sciences* 1970; **7**:561–575.
17. Nelder JA, Mead R. *Computer Journal* 1965; **7**:308.
18. Press WH, Flannery BP, Teukolsky SA, Vetterling WT. *Numerical Recipes*, *The Art of Scientific Computing*. New York: Cambridge University Press, 1986.
19. Albert RA, Rudnicki JW. Onset of shear banding in numerical models of Tennessee marble. EOS, *Transactions of the American Geophysical Union* (Fall Meeting Supplement) 1999; **80**:1055.
20. Albert RA, Rudnicki JW. Non-uniformity of stress and deformation in axisymmetric finite element models of Tennessee marble. NARMS Seattle, WA, July 31–August 2, 2000, submitted for publication.
21. Rice JR. The localization of plastic deformation. In *Proceedings of the 14th International Congress of Theoretical and Applied Mechanics,* vol. I. North-Holland: Amsterdam, 1976.
22. Hill R. The essential structure of constitutive laws for metal composites and polycrystals. *Journal of the Mechanics and Physics of Solids* 1967; **15**:79–95.
23. Olsson WA. The formation of a yield-surface vertex in rock. In *Proceedings of 33rd U.S. Symposium on Rock Mechanics,* Tillerson JR, Wawersik WR (eds). A. A. Balkema: Rotterdam, 1992; 701–705.
24. Storen S, Rice JR. Localized necking in thin sheets. *Journal of the Mechanics and Physics of Solids* 1975; **23**:421–441.
25. Olsson WA. Development of anisotropy in the incremental shear moduli for rock undergoing inelastic deformation. *Mechanics of Materials* 1995; **21**:231–242.

